



Article Processing Dates: Received on 2024-07-11, Reviewed on 2024-09-17, Revised on 2024-10-26, Accepted on 2024-10-26 and Available online on 2024-10-30

Twist and chord optimization using the linearization method on the taper blade of a micro-horizontal axis wind turbine

Muhammad Syaukani^{1*}, Anugrah Wahyu Aryadi¹, Ilham Dwi Arirohman², Sarwo Edhy Sofyan³, Aditiya Harjon Bahar⁴, Sabar⁵

¹Department of Mechanical Engineering, Institut Teknologi Sumatera, Lampung, 35356, Indonesia

²Department of Energy System Engineering, Institut Teknologi Sumatera, Lampung, 35356, Indonesia

³Department of Mechanical Engineering, Universitas Syiah Kuala, Banda Aceh, 23111, Indonesia

⁴Department of Mechanical Engineering, Sampoerna University, Jakarta, 12780, Indonesia

⁵Department of Instrumentation and Automation Engineering, Institut Teknologi Sumatera, Lampung, 35356, Indonesia

*Corresponding author: muhammad.syaukani@ms.itera.ac.id

Abstract

The research aims to optimize the geometry of taper blade profiles for the Horizontal Axis Wind Turbine (HAWT) to improve aerodynamic performance and minimize fabrication complexity. The study used blade linearization as an optimization method for identifying a desirable twist (β) and chord (Cr). This approach enhances accuracy and boosts computational efficiency. It simplifies the optimization process by reducing complexity. In contrast, traditional nonlinear methods are slower and more resource-intensive due to complex aerodynamic interactions. The best β and Cr distributions were found by linearization with elements 1 and 10 of the blade length and positions 5%, 15%, 25%, 35%, 45%, 55%, 65%, 75%, 85%, and 95% of the blade elements. The linearization results were used to determine the optimum performance of the HAWT design using simulation. The optimal blades for HAWT were fabricated and their performance evaluated under real wind conditions. The linearization of the 45% twist and chord of elements 1 and 10 provided the best blade shape. Optimized twist and chord yielded HAWT performance with the C_p of 45% to 47% at rotational speeds of 200–900 rpm and wind speeds of 2–10 m/s. Twist and chord optimization increased the C_p from 39.71% to 46.43% with a rotational speed of 550 rpm at a wind speed of 6 m/s, as well as the maximum mechanical power from 424.28 watts to 500.35 watts at a wind speed of 10 m/s. The result from real wind conditions showed that manufactured HWAT produced an average electrical power of 294.19 watts at a rotational speed of 590.66 rpm. These results demonstrate that the optimized design approach presents a close match and is still reasonable in comparison to practical conditions.

Keywords:

HAWT, twist and chord, linearization, optimization.

1 Introduction

Indonesia primarily relies on non-renewable energy sources, with coal being the most significant. It holds reserves of 38.84 billion tons and produces 600 million tons annually, suggesting a

lifespan of 65 years without new discoveries [1]. However, Indonesia also possesses substantial potential for renewable energy, including 450 MW from mini/micro hydro, 50 GW from biomass, 4.80 kWh/m² per day from solar, 3–6 m/s of wind energy, and 3 GW from nuclear energy [1].

Wind energy is a promising renewable resource in Indonesia, with significant onshore and offshore wind speed distributions shown in Fig. 1. Onshore areas, such as the southern coast of Java and South Sulawesi, experience wind speeds of 6–8 m/s, while offshore locations like the Banten and Sukabumi Seas exceed 8 m/s [2]. The Australian monsoon months of June to August witness these high speeds, while March and April record lower speeds. This possibility highlights the necessity of developing wind turbines to efficiently capture wind energy.

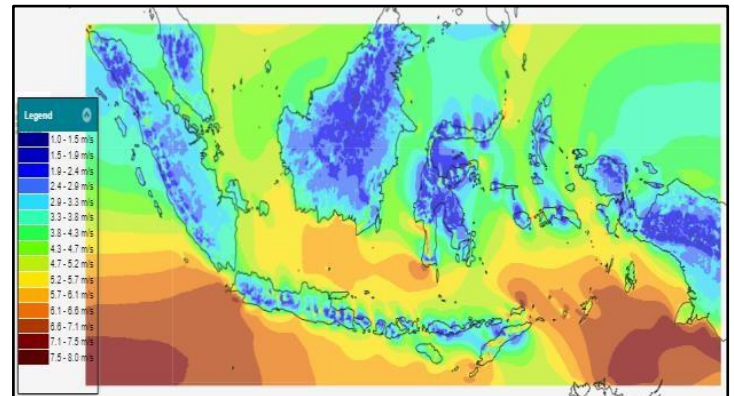


Fig. 1. The distribution of onshore and offshore wind speeds in Indonesia [2].

Through the rotation of the rotor and generator shaft, wind turbines convert wind kinetic energy into mechanical energy, which then transforms into electrical energy. Wind turbines can effectively harness wind energy at speeds ranging from 1.6 m/s to 3.3 m/s for minimum operation and from 13.9 m/s to 17.1 m/s for the highest limit of electrical power generation [4]. A micro-scale wind turbine, suitable for Indonesia, can generate up to 50 kW with a construction area of around 200 m². These turbines operate at wind speeds of 4.0 to 4.5 m/s and have sizes ranging from 1 to 7.5 meters [5,6]. Designing turbine blades that adapt to Indonesia's wind conditions is essential for optimal performance.

The airfoil design largely determines the efficiency of wind turbine blades. Saputro and Rumakso [7] used QBlade software to analyze blade performance by modifying the airfoil, finding that each airfoil has distinct lift and drag coefficients, unaffected by wind speed. Wahyudi *et al.* [8] studied NACA 3612 airfoils on taper, taperless, and inverse taper blades, showing that taperless blades with two blades produced a maximum power output of 0.846 watts at a wind speed of 6.11 m/s.

Material selection is crucial in wind turbine blade design. Ikaningsih and Rosihan [9] found that using styrofoam at the blade's middle and tip helps prevent overspeed at high wind speeds. Large-scale blades commonly use carbon fiber composites due to their high bending stress value around 207.48 MPa, which makes them durable for long-term use in capturing wind energy [10].

Micro-scale wind turbines commonly use fiberglass and wood composites for their blades. Fiberglass's strength depends on its fiber pattern [11], while wood is abundant in Indonesia, with materials like teak, mahogany, and pine offering unique properties. Studies using the DIN standard show pine wood has static bending strengths around 62,400 kg/cm² [12,13]. Rangkuti *et al.* [14] simulated pine wood in tapered blades and found a maximum stress of 5.295 MPa, a deflection of 9.102 mm, and a safety factor of 7.743.

The simplicity of the turbine blade manufacturing process is crucial when selecting materials and airfoils for micro-scale wind

turbines. Prioritizing easily manufactured materials is crucial as complex designs increase costs. Blade geometry complexity also impacts production and optimization techniques help simplify the process while achieving optimal turbine performance.

Recent studies introduced mathematical and numerical methods to optimize blade geometry for improved aerodynamic performance. Jieyan, Chen *et al.* [15] summarized optimization techniques like Sequential Quadratic Programming (SQP), Genetic Algorithms (GA), Particle Swarm (PSA), and Coral Reef Optimization (CRO). Selig [16] used GA to optimize chord length and twist angle, maximizing energy production. Ceyhan [17] combined GA with BEM theory, while Liu and Chen [18] improved AEP by 7.5% using a compact GA. Abbaskhah [19] used Multilayer Perceptron (MLP) and Convolutional Neural Networks (CNN) for HAWT optimization, but these models didn't account for the linearization of chord and pitch angle distribution, which is now a key industry need.

Sedaghat *et al.* [20] found that a modified linear rotor underperformed compared to the original shape. In contrast, Ramazan and Mustafa [21] achieved excellent results with a novel artificial bee colony algorithm for optimizing small-scale turbine blades. Jian Xu *et al.* [22] showed that the CNN-BEM model quickly and accurately predicted tidal turbine performance. Using the Betz-Joukowski Limit theory, Kale *et al.* [23] improved the performance of microturbines by 30%. Keshavarzadeh *et al.* [24] created a BEM framework for optimizing rotor shape and suggested that blade loading should be increased to reduce AEP sensitivity. Rahgozar *et al.* [25] found non-linearized micro-scale blades produced better power output but had starting issues. Abdelsalam *et al.* [26] noted similar power coefficients between linearized and original blades, but the original struggled below 5 m/s. Augustiantyo and Setiawan [27] revealed that a taper blade with the SELIG 6043 airfoil achieved a C_p value of 52.2% when linearized at a 75% chord range and 55% twist range.

The aforementioned studies emphasize the need for further research on simple blade linearization, as quantitative evaluations of linearized wind turbine blade performance are limited. This optimization method improves the accuracy of computations while

keeping them efficient. It makes the process easier compared to traditional nonlinear methods, which need a lot of computing power and take longer to converge because aerodynamic forces are so complicated. This research addresses a gap by illustrating how the combination of the Blade Element Momentum (BEM) method and simple linearization can enhance aerodynamic performance and energy efficiency in small-scale, low-wind-speed microturbines.

The linearization method was employed to optimize the twist angle and chord length of wind turbine blades, which are critical for performance. Initially designed using the BEM method, the blades were modified by linearizing each element to achieve an optimal distribution of twist and chord along the blade. The resulting geometry is then assessed for aerodynamic performance before proceeding to manufacture the blades and create a 3D model of the wind turbines. Finally, the constructed pine wood turbines will be tested to validate their design performance.

2 Research Method

This study aims to optimize the taper blade geometry of horizontal axis wind turbines for improved aerodynamic efficiency and energy output. We employed blade linearization to minimize variations in twist and chord values, thereby simplifying the design and production processes. Initially, the characteristic analysis of several airfoils was generated using QBlade software to establish the blade's cross-section.

The original blades served as a reference for modifications based on linearization results to evaluate the aerodynamic performance. By making the blade elements linear between 5% and 95%, including elements 1 and 10, the modified blades generated the best twist (β) and chord (Cr) distributions. The study also evaluated the blade design performance at average wind speeds in Indonesia (2 to 10 m/s) to estimate the potential maximum mechanical power output and predict micro-wind turbine performance. We manufactured and 3D modeled the blades before testing them to confirm their effectiveness in generating electrical power under real wind conditions. Fig. 2 illustrates the research methodology in detail.

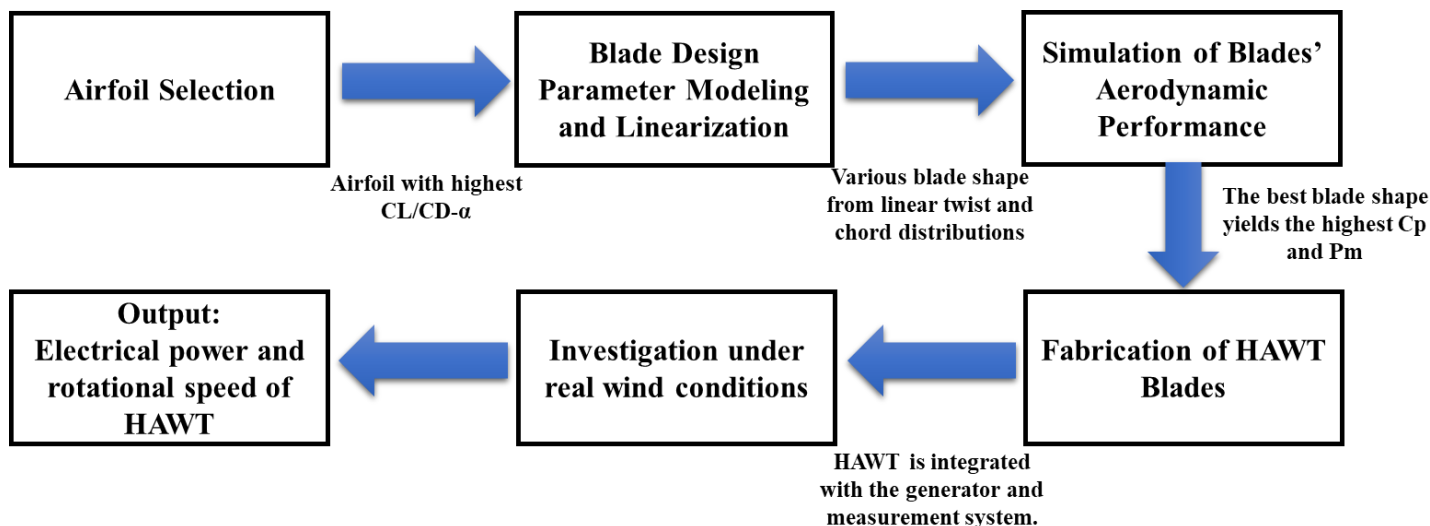


Fig. 2. Flowchart of taper blade optimization for HAWT.

2.1 The BEM Theory Using QBlade

HAWT performance design and modeling were done using a QBlade, a free software for wind turbine blade design and simulation under various wind conditions. It offers a practical platform for analyzing aerodynamic performance without the need for external data processing. QBlade supports airfoil design, lift and drag analysis, blade optimization, and turbine simulation. Users can choose between HAWT, Vertical Axis Wind Turbine (VAWT), and propeller designs. For HAWT design and modeling, the user can select the HAWT mode for providing rotor blade

design, rotor BEM simulation, turbine BEM simulation, and multiparameter BEM simulation. The main menu of QBlade Software is displayed in Fig. 3.

In QBlade, aerodynamic forces operating on a rotor may be described using a steady BEM or a more sophisticated method. This study used a mathematical model based on one-dimensional BEM theory. A rotor may be described as a one-dimensional permeable disk. The disc is deemed perfect since it is frictionless and has no rotational velocity component in its wake.

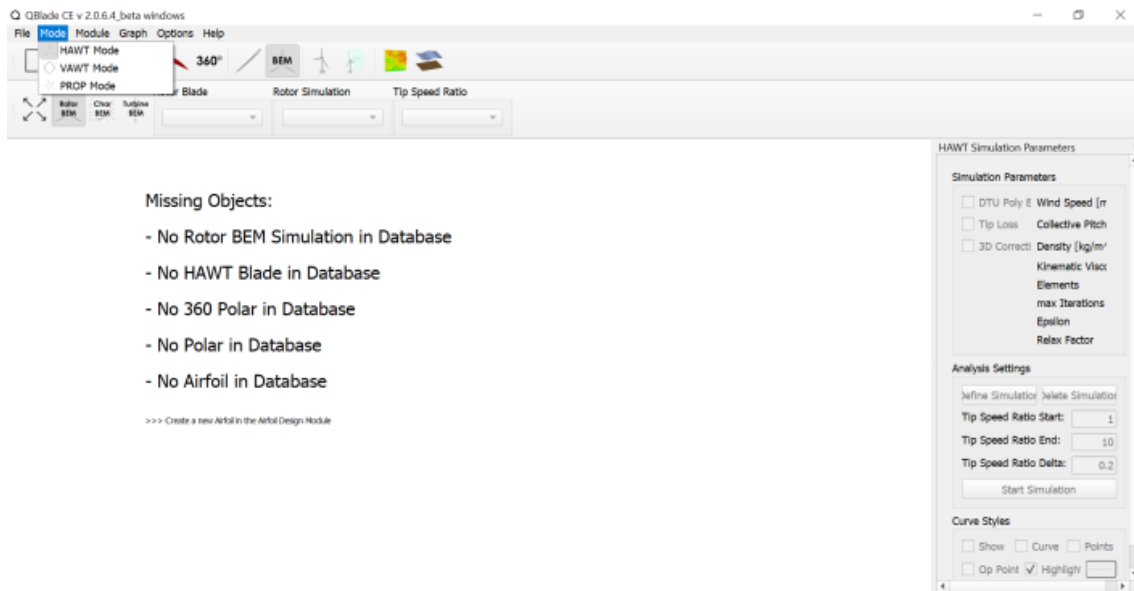


Fig. 3. The main menu of QBlade.

Fig. 4 illustrates one-dimensional momentum theory, pressure, and velocity at the rotor or wind turbine. The Bernoulli equation was employed for this case [29]. These assumptions allow the use of mass and momentum conservation to calculate rotor performance (power and thrust) and velocity in the rotor plane. The induction factor (a) relates the rotor plane velocity (U) to the incoming velocity (U_0) as formulated in Eq. 1-Eq. 2 [28].

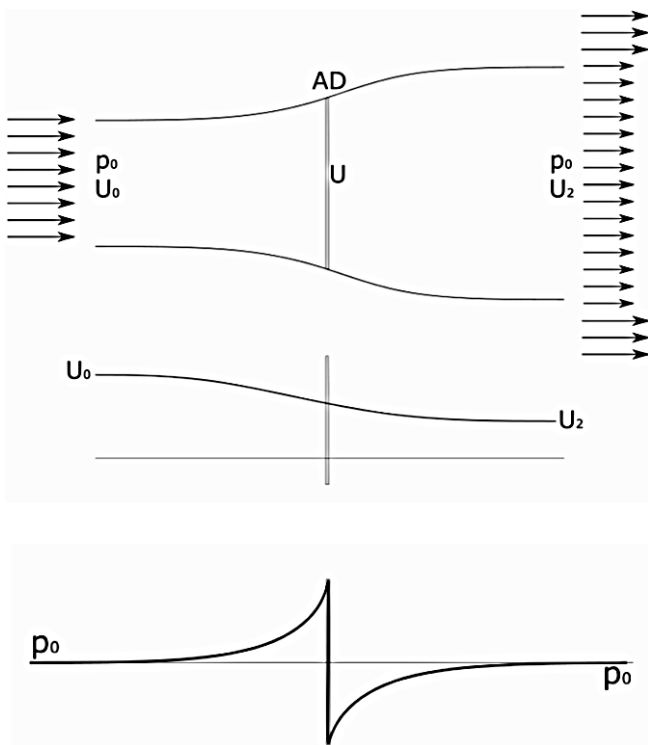


Fig. 4. One-dimensional momentum theory, pressure, and velocity [28].

$$\Delta p = \frac{1}{2} \rho (U_0^2 - U_2^2) \quad (1)$$

$$U = (1 - a)U_0 \quad (2)$$

Rotor performance coefficients for power and thrust, C_p and C_T , can alternatively be described in terms of the axial induction factor (a) through Eq. 3-Eq. 4 [28].

$$C_T = 4a(1 - a) \quad (3)$$

$$C_p = 4a(1 - a)^2 \quad (4)$$

2.2 Airfoil Selection

Previous studies have focused on airfoil performance by determining drag and lift coefficients numerically or experimentally under various flow conditions. Yamin and Zaid [30] evaluated several NACA airfoils to predict airfoil performance by machine learning. The initial step in developing wind turbine blades was to examine airfoil characteristics. The airfoil utilized must be of high performance and capable of producing a greater lift force than drag to produce an optimal performance of the wind turbine. The airfoils investigated include the WORTMANN FX 76-120, Falcon, NACA 2410, E186, and SELIG 3002 to investigate coefficient lift (C_L) and the ratio of coefficient lift to coefficient drag (C_L/C_D) with respect to angle of attack (α). Airfoil geometry profiles were selected in this study as shown in Fig. 5.

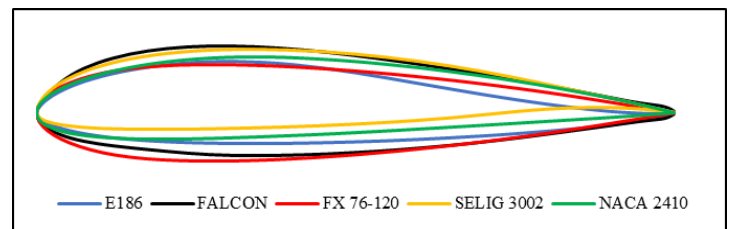


Fig. 5. Geometry profile of selected airfoils.

2.3 Blade Design Parameter Modeling and Linearization

Table 1 displays the design parameters of the micro-scale HAWT blade. We used these variables to determine the optimal twist and chord for the design operational conditions. Eq. 5–Eq. 9 provided the twist and chord of each element for the original blades as the basis. The modified blades achieved optimal twist (β) and chord (Cr) distributions by linearizing the blade elements (5%, 15%, 25%, 35%, 45%, 55%, 65%, 75%, 85%, and 95%), as well as elements 1 and 10 along the blades.

Table 1. Design parameters of HAWT blade

Parameter	Value
Blade type	Taper
Maximum blade chord length	0.12 m
Number of blade elements	10
Blades number	3
Rotor radius	0.8 m
Hub radius	0.17 m
Tip speed ratio (λ)	7
Maximum wind speed	10 m/s

Analysis of twist (β) and chord (C_r) on each blade element is necessary when using BEM theory for blade geometry design. Identifying the partial radius (r), partial tip speed ratio (λ_r), chord length (C_r), and flow angle (ϕ) are some crucial modeling factors. The mathematical modeling of this study is represented in Eq. 5-Eq. 12 [31].

The partial radius (r), which indicates the distance or location of the blade element from the base point, is formulated by Eq. 5. R is the length of the blade in meters, and n is the number of blades.

$$r = 0.22 + \left[\left(\frac{R-0.22}{n} \right) \times \text{total element} \right] \quad (5)$$

The partial tip speed ratio (λ_r) is calculated from the overall tip speed ratio on the wind turbine rotor, as shown in Eq. 6.

$$\lambda_r = \frac{r}{R} \times \lambda_R \quad (6)$$

C_r is the length of the chord calculated from the number of blades used and the Coefficient Lift (C_L) obtained from the simulation of the characteristics of the airfoil (Eq. 7).

$$C_r = \frac{16\pi \times R \times \frac{R}{r}}{9\lambda^2 \times n \times C_L} \quad (7)$$

$$\phi = \frac{2}{3} \tan^{-1} \frac{1}{\lambda_r} \quad (8)$$

ϕ is the flow angle, which is the parameter to be used to determine the twist angle (β) of the HAWT blade, as shown in Eq. 9.

$$\beta = \phi - \alpha \quad (9)$$

The amount of mechanical power, P_m (watts), generated depends on the torque, T (Nm), and rotational speed, ω (rpm) of the wind turbine rotor. The value of wind turbine performance is formulated using Eq. 10.

$$P_m = T \times \omega \quad (10)$$

Coefficient of power (C_p), as shown in Eq. 11, refers to the amount of wind power potential that can be converted to mechanical power of a wind turbine. It depends on the sweep area of the wind turbine, A (m²), and wind speed flow through the wind turbine, V (m/s).

$$C_p = \frac{P_m}{\frac{1}{2} \rho A V^3} \quad (11)$$

The electrical power of the wind turbine, P_e (watts), will be calculated using Eq. 12 from the value of mechanical power multiplied by several parameter efficiencies: generator efficiency (η_{gen}), transmission efficiency (η_{tr}), and controller efficiency (η_c).

$$P_{el} = \eta_{gen} \times \eta_{tr} \times \eta_c \times P_m \quad (12)$$

2.4 Simulation of Aerodynamic Performance

The aerodynamic performance analysis came after linear optimization was used to find the modified blades' linear twist and chord distribution. QBlade software simulated the modified geometry to identify optimal C_p , mechanical power (P_m), and torque based on $\lambda = 1-10$ and the wind turbine's rotational speed. The study also evaluated the blade design's performance at average wind speeds in Indonesia, varying between 2 and 10 m/s, to estimate the potential maximum mechanical power generated and provide a prediction of micro-wind turbine performance.

2.5 Experimental Analysis

The designed turbine, featuring three blades optimized through linearization, was further tested. The blades, made from pine wood, were manually manufactured. Additional field testing is necessary to validate the simulation data. Fig. 6 shows the experimental setup, which includes a microwind turbine and measurement instruments. A three-phase magnetic cogging-less generator is used to generate electrical power. The measuring system consists of a laser tachometer, multimeter, anemometer, data logger, and PC for monitoring wind speed, rotational speed, and electrical current and voltage. Testing was obtained at 5 meters above ground, collecting hourly data on electrical power and rotational speed for 24 hours.

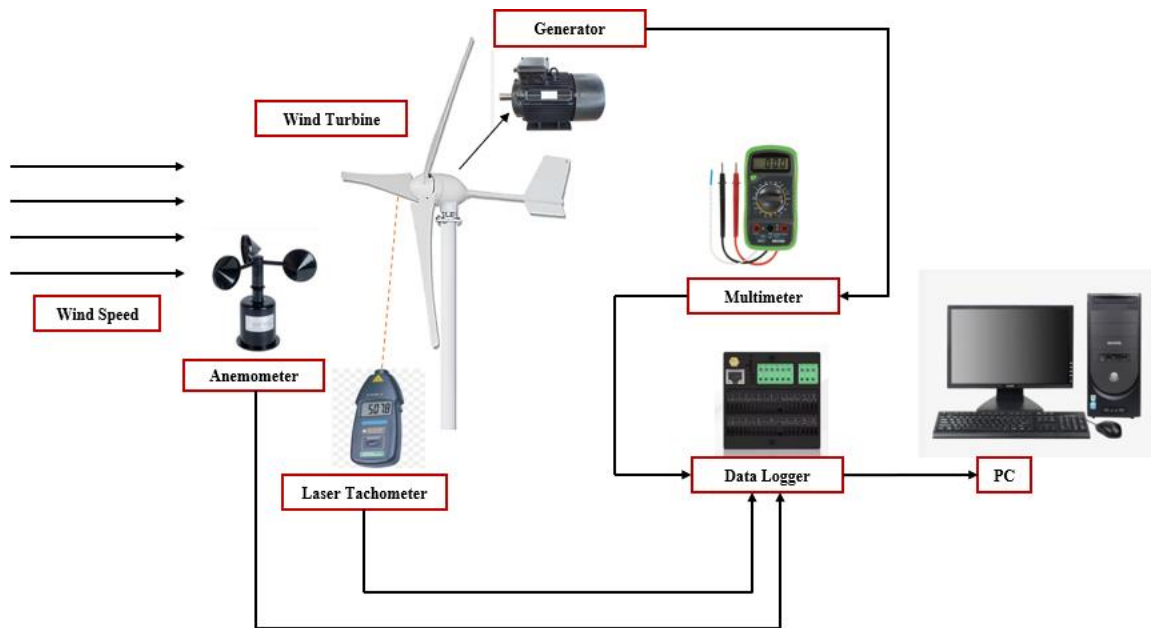


Fig. 6. Experimental setup.

2.6 Uncertainty Analysis

The instrument uncertainties were used to calculate the percentage uncertainties of rotational speed, wind speed, electrical current, voltage, and data logger system. Table 2 displays the uncertainties for rotational speed (ω), wind speed (v), electrical current (I), voltage (V), and data logger system (DL), which were

$\pm 2\%$, $\pm 1\%$, $\pm 1\%$, and ± 1 , respectively. The overall uncertainty was computed with Eq. 13. The error propagation approach employed in this investigation was based on earlier research [32]. The overall uncertainty was less than 5%, indicating that the testing results in this study were statistically reliable.

$$\text{Total Uncertainty} = \sqrt{(\omega)^2 + (v)^2 + (I)^2 + (V)^2 + (DL)^2} \quad (13)$$

$$\text{Total Uncertainty} = \sqrt{(2\%)^2 + (2\%)^2 + (1\%)^2 + (1\%)^2 + (1\%)^2} = \pm 3.31\%$$

Table 2. Uncertainty of the instruments employed in this study

Parameter	Percentage of uncertainty	Measurement technique
Rotational speed of wind turbine	±2%	Laser tachometer
Wind speed	±2%	Anemometer
Electrical current	±1%	Digital multimeter
Electrical voltage	±1%	Digital multimeter
Data recorder	±1%	Data logger

3 Results and Discussion

3.1 Airfoil Selection Result

Fig. 7 illustrates the relationship between C_L - α C_L/C_D - α from different airfoils. Generally, SELIG 3002 has the greatest value of C_L at different α from 2 to 12 degrees. The WORTMANN FX 76-120 airfoil had an optimal C_L/C_D value of 70.08 at α value of 8. The optimal C_L/C_D for Falcon is 87.9 with a α value of 8, while the optimal C_L/C_D for the NACA 2410 is 95.38 with a α value of 4.5. The E186 airfoil had an optimal C_L/C_D value of 64.55 at α of 3.5. The SELIG 3002 had an optimal C_L/C_D of 105.32 with an α value of 5.5.

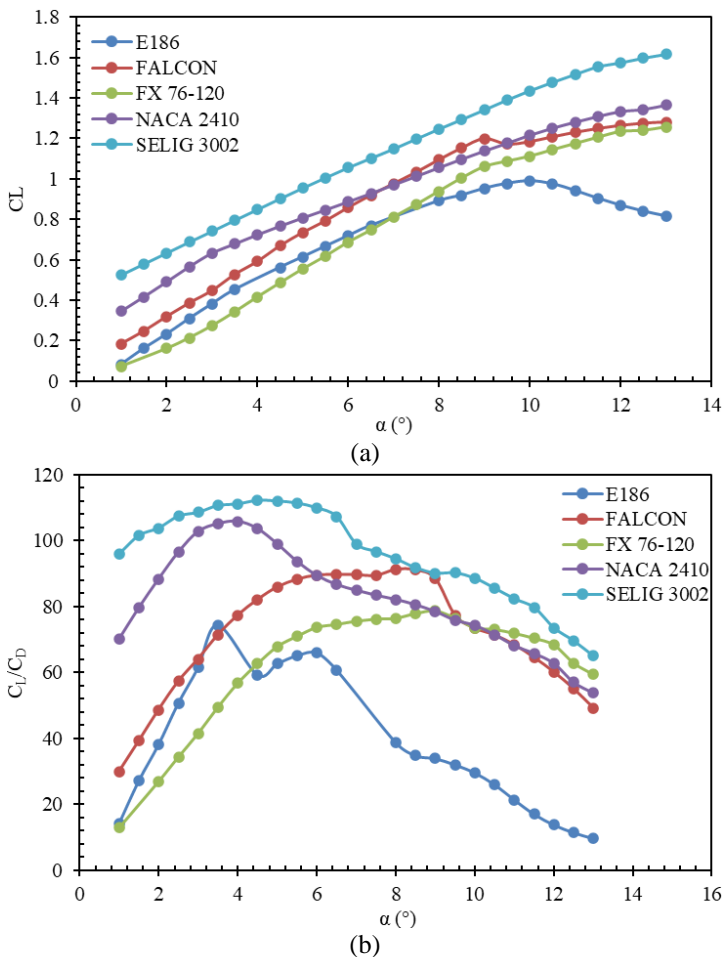


Fig. 7. Relationship between (a) C_L - α , (b) C_L/C_D - α different airfoils.

The findings on the airfoil characteristics revealed that the value of C_L/C_D increases as the α value increases until it reaches an optimal value for each airfoil. This value will decrease once it has exceeded the optimal α value as a result of fluctuating air flow and turbulence. A stall occurs when the C_L/C_D levels decrease after achieving the optimal α value [33]. Higher α does not usually

imply higher C_L/C_D values. When the lift pressure is lower than the dynamic pressure of the fluid flow across the airfoil, the C_L/C_D ratio is lower. This is caused by the negative wind direction. A negative C_L/C_D ratio, as reported by Pranesh et al. [34], indicated that the blade is rotating opposite the axis. The examination of airfoil characteristics using QBlade led to the selection of SELIG 3002 as the ideal airfoil for wind turbine designs.

3.2 Linearization of Blade Geometry Design

Table 3 shows the initial value of twist and chord (baseline) of elements 0 through 10 against partial TSR (λr) or partial radius (r) calculated using Eq. 5-Eq. 9. The distribution of twist and chord of blade geometry became the references for the linearization process.

Table 3. Twist and chord baseline

Element	r (m)	β (°)	C_r (m)
0	0.17	22.108	0.143
1	0.233	16.919	0.104
2	0.296	13.574	0.082
3	0.359	11.272	0.068
4	0.422	9.602	0.058
5	0.485	8.34	0.05
6	0.548	7.353	0.044
7	0.611	6.563	0.04
8	0.674	5.916	0.036
9	0.737	5.376	0.033
10	0.8	4.92	0.03

Linearization was next employed in blade geometry optimization to attain the optimum β distributions. Fig. 8 displays the result of that throughout all the linearization intervals. The twist value tended to rise from the tip section at its maximum partial radius to the root section of the blade. Despite a linearization of 5% across two points (elements 0 and 1), the twist increases substantially at 0.17 m in comparison to the value at the tip section. Throughout the linearization interval, the characteristic twist slope decreases. Consequently, for every linearization interval between 5% and 95%, the highest and lowest twists will be smaller, as concluded in Table 3. The highest and lowest values of linear twist were 22.11° and 29.79° , both obtained from the linearization of 5%. Each element had a maximum twist difference of 5.19° at 5% linearization and a minimum twist difference of 0.46° at 95% linearization. The twist variation of each blade element remained exactly the same for any percentage of linearization. The result suggests an effective implementation of the twist linearization technique as the foundation for the blade's geometrical optimization.

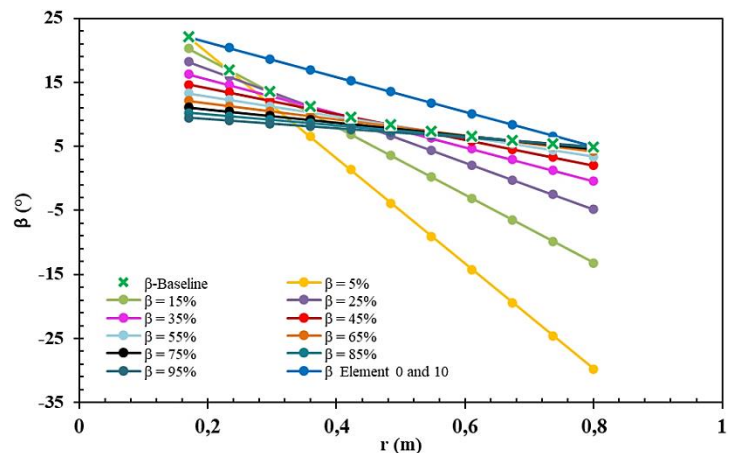


Fig. 8. Comparison of twist distributions from linearization 5%–95%, elements 1 and 10 of the blade.

A negative twist value denotes, as shown in Table 3, a significant twist change along the blade. Developing a blade that

has negative twist distribution is difficult because it necessitates a complicated manufacturing process, specific materials, and hefty costs [35]. Likewise, the linearization of twist ranges from 5%–35% and was ineligible for modeling with QBlade software based on the BEM method. As a result, the linearization proceeds from 45% to 95%, and the elements 1 and 10 were chosen to further identify the optimal power coefficient (C_p).

Fig. 9 shows the graph of chord length linearized between 5% and 95% and elements 1 and 10. The characteristics of the chord linearization result had similarities with twist. The largest linear slope also occurred on a 5% chord linearization. The largest chord value was 0.143 m, and the smallest, -0.244 m, occurred at linearization in the 5% range, as in Table 4. The highest and lowest chord value differences for each element were 0.039 and 0.003 at 5% and 85%–95%, respectively.

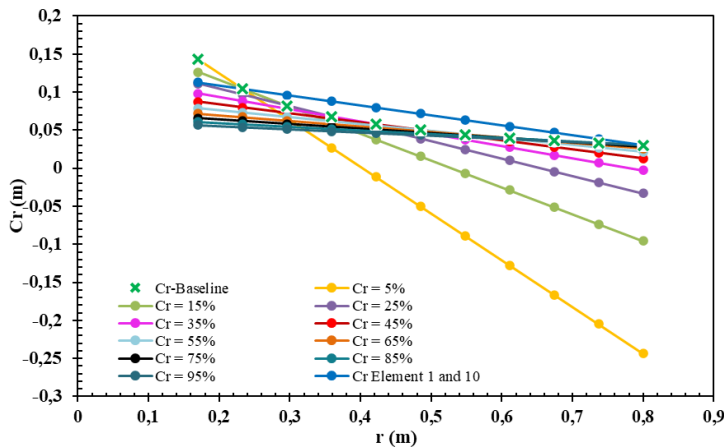


Fig. 9. Comparison of chord length distributions from linearization 5%–95%, elements 1 and 10 of the blade.

Table 4. Result of twist linearization

Twist of blade element (%)	Linearized of β ($^\circ$)		$\Delta\beta$ ($^\circ$) linear each element	Result
	Highest	Lowest		
$\beta = 5$	22.11	-29.79	5.19	-
$\beta = 15$	20.26	-13.18	3.34	-
$\beta = 25$	18.18	-4.84	2.30	-
$\beta = 35$	16.28	-0.42	1.67	-
$\beta = 45$	14.65	2.03	1.26	✓
$\beta = 55$	13.27	3.41	0.99	✓
$\beta = 65$	12.10	4.19	0.79	✓
$\beta = 75$	11.09	4.62	0.65	✓
$\beta = 85$	10.23	4.84	0.54	✓
$\beta = 95$	9.48	4.92	0.46	✓
β element 1 and 10	22.11	4.92	1.72	✓

Xu et al. [36] investigated how the chord distribution affected the shape of the blade employed, from the base end to the tip section. To determine the appropriate chord length for the specified blade design, one must determine the chord's linearity to align with the size of the turbine under construction. Table 5 determined the maximum chord length in the present investigation to be 0.12 m. Therefore, we selected corresponding chord distributions based on the linearization of elements 1 and 10, where the highest linear chord value was 0.113 m at a partial radius of 0.17 m across the blade's root section, and the lowest chord value was 0.03 m at the tip section.

3.3 Analysis of Performance Optimized Blade Design

The simulation results of C_p with respect to λ are shown in Fig. 10. Typically, the C_p for the 45% to 95% of twist is larger than for twist elements 1 and 10. A linear twist of 55%–95% had an identical C_p on each $\lambda = 1$ –10. The 45% twist linearization range might generate the highest C_p compared to others, such as at $\lambda =$

5–10. In addition, the maximum C_p was 46.45% for 45% of the twist linearization range with an average value of $\lambda = 7.5$. The C_p increases as λ increases to the maximum point, then decreases to 10 of λ . This happens due to λ being linear in comparison to the rotational speed of the blade. λ is the ratio of the rotational speed multiplied by the rotor radius to the wind speed. The higher the speed of rotation of the wind turbine blade, the greater the power generated. However, high rotational speeds do not instantly indicate high efficiency [37], [38], as these may result in losses due to increased drag force and higher turbulence intensity, which result in the disruption of airflow around the blades [8], [38].

Table 5. Result of chord length linearization

Chord length of blade element (%)	C_r linear (m)		ΔC_r linear each element (m)	Result
	Highest	Lowest		
$C_r = 5$	0.143	-0.244	0.039	-
$C_r = 15$	0.126	-0.096	0.022	-
$C_r = 25$	0.111	-0.033	0.014	-
$C_r = 35$	0.098	-0.003	0.010	-
$C_r = 45$	0.088	0.013	0.007	-
$C_r = 55$	0.079	0.021	0.006	-
$C_r = 65$	0.072	0.026	0.005	-
$C_r = 75$	0.066	0.029	0.004	-
$C_r = 85$	0.061	0.030	0.003	-
$C_r = 95$	0.056	0.030	0.003	-
C_r element 1 dan 10	0.113	0.030	0.008	✓

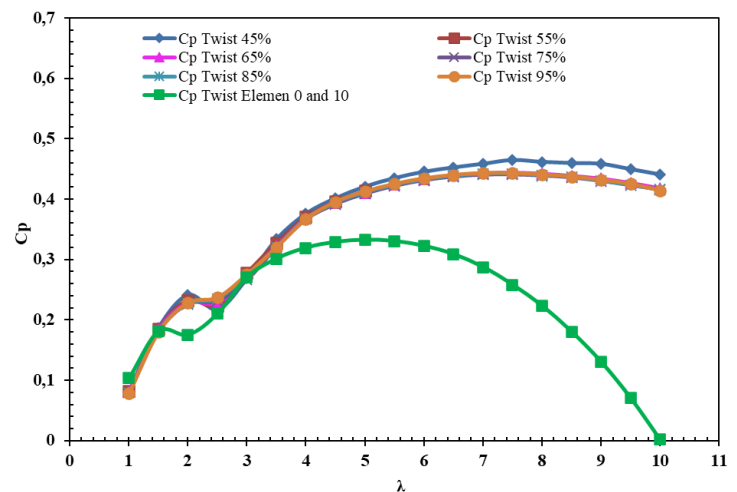


Fig. 10. Relationship C_p corresponding to TSR with linearization of twist 45%–95%, elements 1 and 10.

Fig. 11 illustrates the analysis of the torque that wind turbine blades generate. Torque is a force that makes the blade rotate or move in a circular motion around its axis. The magnitude of the generated torque had a significant impact on the power coefficient and performance of the proposed wind turbine. The torque increased from $\lambda = 1$ to reach optimal values on $\lambda = 2$ for the entire twist range of 45%–95% and elements 1 and 10. Subsequently, the torque decreased significantly as the λ value increased to reach the minimum condition at $\lambda = 10$. This occurs as a consequence of the increasing mechanical losses to the blade turbine caused by the constant rise in the rotational speed of blades [8], [39].

Typically, linear twisting in the 45%–95% range produced a better torque distribution against λ than elements 1 and 10. Similarly, the effect of twist linearization in the 45%–95% twist range showed little impact on torque with $\lambda = 1$ –10. Therefore, we selected a linear twist of 45% and linear chord elements of 1 and 10. This was based on the analysis of its effect on the power coefficient that can be generated by the blades, which was 46.45%. Fig. 12 illustrates the comparison between the blade design baseline and after optimization.

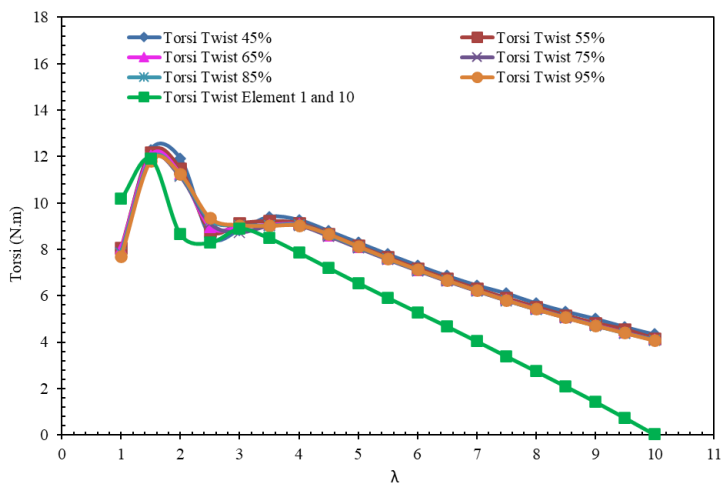


Fig. 11. Relationship torque corresponding to TSR with the linearization of twist 45%–95%, elements 1 and 10.

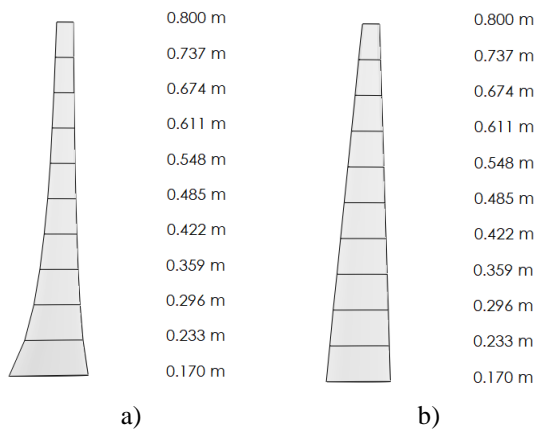


Fig. 12. Blade profile design a) baseline, b) optimized blade.

3.4 Performance Analysis of Wind Turbine Rotor

Fig. 13 illustrates the impact of tip speed ratio (λ) from 1 to 10 on the power coefficient (C_p) at wind speeds of 1 to 10 m/s. Generally, as λ increased, C_p rose until reaching an optimal point, after which it declined at $\lambda = 10$. As wind speeds exceed the optimal range, blades face aerodynamic inefficiencies like increased drag and turbulence. The unstable airflow can cause flow separation, reducing lift and efficiency [40], [41]. This led to a drop in the coefficient of power (C_p). The simulation also indicated that variations in wind speed had minimal effect on C_p , suggesting that the turbine blades were capable of maximizing power output despite changing wind conditions. In Indonesia, where average wind speeds range from 6 to 8 m/s, the power coefficient at $\lambda = 7.5$ was 46.43%, indicating that the blade design was well-suited for optimal performance in these conditions. The generation of power determines the optimal performance of a wind turbine. The rotational speed and torque produced by the wind turbine blades are key factors that determine the amount of power generated.

Fig. 14– Fig.15 illustrates how rotational speed affects C_p and torque when wind speed varies by 1–10 m/s. In fact, a desirable rotating speed for each wind speed yielded the highest C_p . Considering the wind speed of 6 m/s, an optimal rotational speed of 550 rpm yielded a C_p of 46.43%. In such operating conditions, the wind turbine designed with a maximum torque of 8.69 Nm may generate the highest power when the wind speed reaches 10 m/s (Fig. 15). At a torque of 2.14 Nm and a wind speed of 6 m/s, the wind turbine generated the minimum power. The turbine operates efficiently across various rotational speeds depending on wind speed, but efficiency drops after a certain point for each wind speed curve. At higher wind speeds, aerodynamic issues like stalling, flow separation, and increased drag reduce performance, causing a decrease in C_p [40], [41]. Every wind speed possesses an optimal rotational speed that maximizes torque. As rotational

speed increases, the interaction between the blades and wind becomes less efficient, leading to a torque drop [42]. At a fixed 550 rpm, drag forces became more significant than lift, reducing net torque, especially at higher wind speeds.

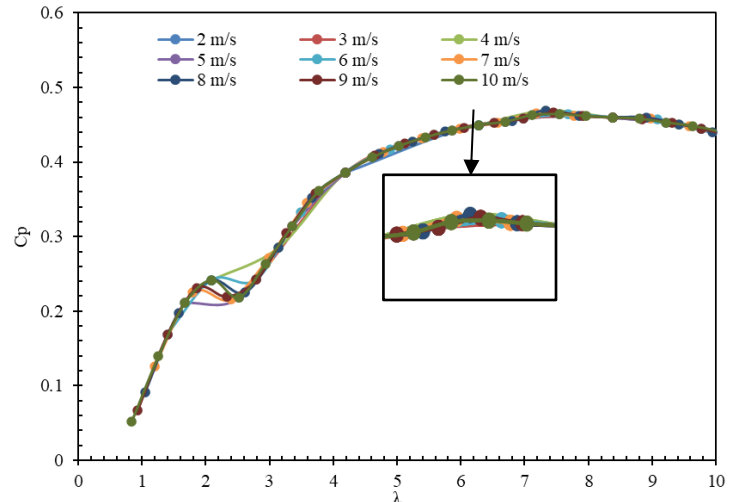


Fig. 13. The coefficient of performance (C_p) relates to TSR at wind speeds of 1–10 m/s.

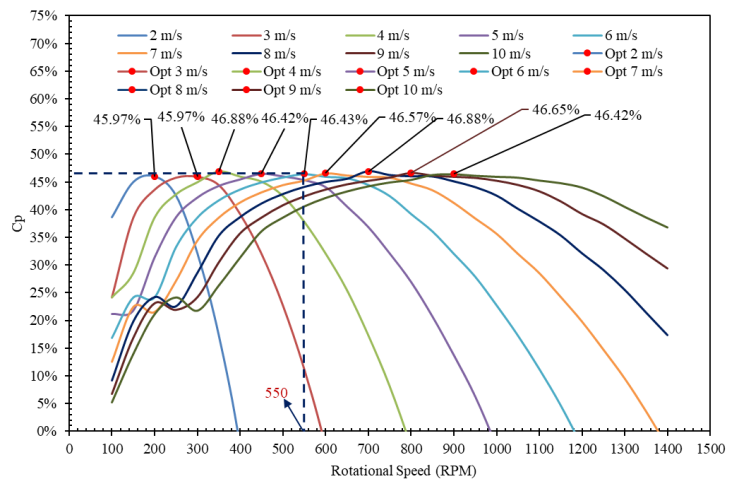


Fig. 14. The coefficient of performance (C_p) relates to rotational speed at wind speeds of 1–10 m/s.

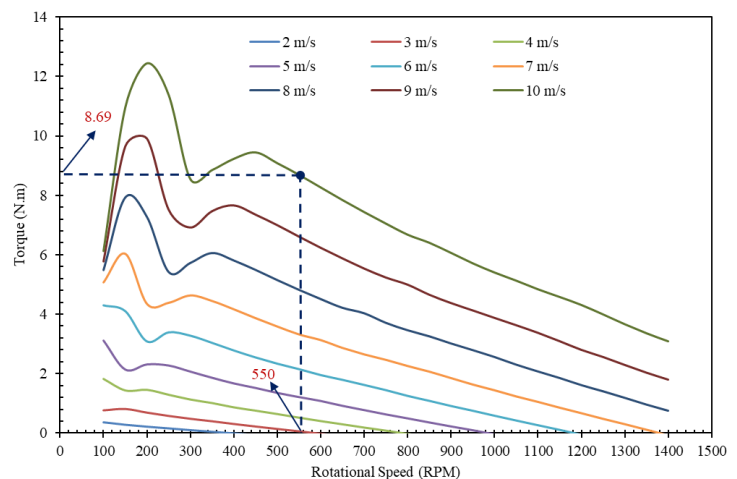


Fig. 15. Relationship torque and rotational speed at wind speeds of 1–10 m/s.

Fig. 16–Fig. 17 shows the difference in aerodynamic performance between the optimized blade and the baseline, as shown by the coefficient of performance (C_p) and the mechanical power output (P_m). For variations in wind speed of 3–10 m/s, the overall optimized blade was above the baseline blade [21], [27], [43]. At a wind speed of 6 m/s, the optimized blade's C_p increased to 46.43% from the baseline value of 39.71%. Furthermore, the

generated power began to rise at a wind speed of 4 m/s and increased significantly to reach 10 m/s. Optimizing the blade geometry resulted in an average increase in C_p of 6.7%, regardless of the wind speed.

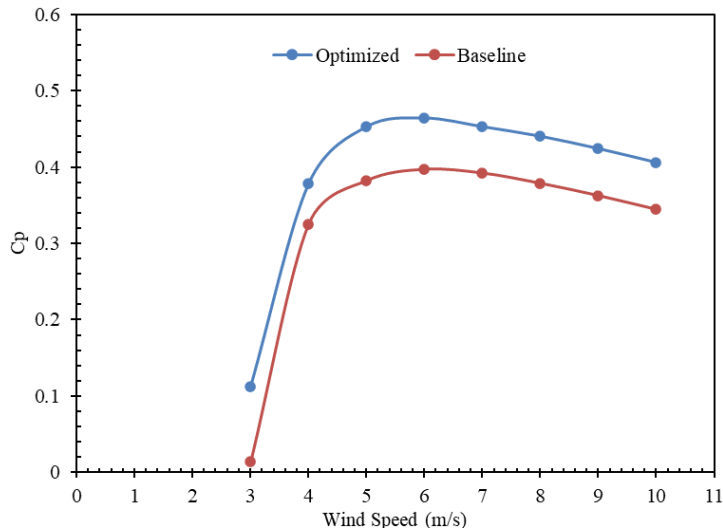


Fig. 16. Relationship C_p and wind speed of baseline and optimized blades.

The greatest mechanical power that an optimized blade can produce is 500.35 watts, whereas the maximum baseline mechanical power is around 424.48 watts at a speed of 10 m/s. Furthermore, at a wind speed of 6 m/s, both the baseline and the optimized blade can generate mechanical power of 105.62 watts and 123.5 watts, respectively. Therefore, the process of optimizing the blade geometry based on the twist and chord parameters greatly impacted the performance of the turbines, resulting in an increase in electrical power of 17.87% and 16.93% at wind speeds of 10 m/s and 6 m/s, respectively. The optimization of blade geometry resulted in an average increase in mechanical power of 16.95%, regardless of the wind speed.

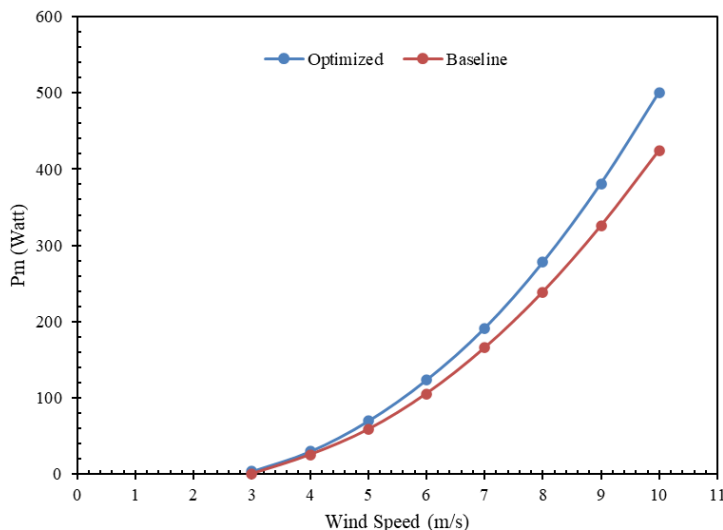


Fig. 17. Mechanical Power (P_m) corresponding to wind speed of baseline and optimized blades.

3.5 Experimental Analysis

Fig. 18 shows the manufactured wind turbine model in this study, ready for performance tests. Pine wood was the material utilized. Wind turbine testing was carried out at a height of 5 meters above the ground in real wind conditions. Real wind conditions involve unpredictable and naturally varying wind speeds, directions, and turbulence that occur outdoors. The experiment collected data on the electrical power and rotational speed generated hourly for 24 hours, as shown in Fig. 19. The testing process began at 8:00 AM, recording the maximum

electrical power output and rotational speed hourly for 24 hours. The turbine produced 294.19 watts of power at its highest capacity. While the greatest rotational speed achievable was 590.66 rpm, this value was not significantly different from the simulation, which was 550 rpm with an average wind speed of 6 m/s and the highest C_p of 46.43%.



Fig. 18. Manufactured HAWT blades.

The findings also showed that the wind turbine reached its maximum output between 3:00 and 5:00 PM, and it actively generated electricity from 7–12 hours, specifically from 2:00 PM to 8:00 PM. The turbine did not generate electricity from the 16th to 21st hours. Previous studies [44]–[46] also showed that the maximum average daily wind power potential in Indonesia occurs during this time, reaching its highest between 2:00 PM and 6:00 PM.

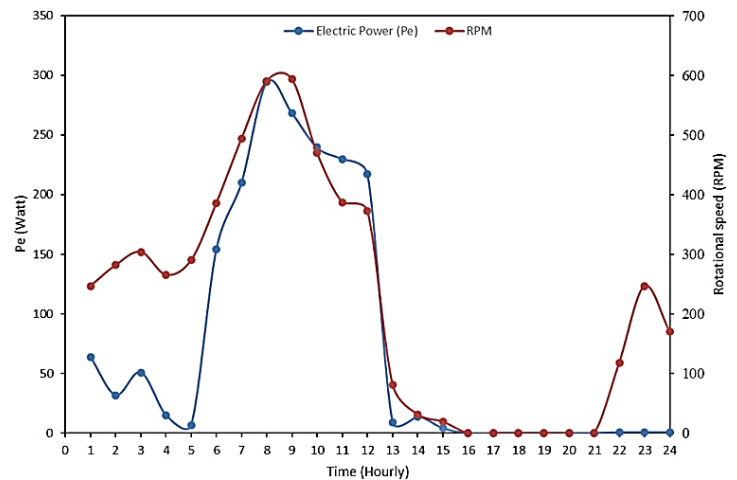


Fig. 19. Experimental data on mechanical power rotational speed with respect to time (hourly).

3.6 Comparative analysis and Validation Results

It is necessary to compare the designed wind turbine performance simulation results with the experimental wind turbine performance. The power generated is a comparable parameter. In order to calculate the power using simulation, a few operating parameters need to be established, as indicated in Table 6. In this study, transmission efficiency and controller efficiency are determined to be 90%. However, the efficiency of the generator cannot be confirmed. Thus, additional testing is required to evaluate the performance of the generator type employed. Consequently, in order to determine its impact on the power produced, generator efficiency is included as an independent variable in sensitivity analysis. Assume that the generator that is being used has an efficiency range of 70%–90%. Sensitivity analysis helps predict wind turbine aerodynamic performance by identifying how changes in variables, like wind speed or blade angle, affect power generation, as investigated by previous studies [47], [48].

Table 6. Operation parameters for simulation and experiment validation

Operation parameter	Value
Cut in wind speed	3 m/s
Cut off wind speed	25 m/s
Average wind speed	6 m/s
Generator efficiency	70%-90%
Transmission efficiency	90%
Controller efficiency	90%

The mechanical power is multiplied by the system efficiency to produce the simulated power. In order to calculate system efficiency, multiply the controller, generator, and transmission efficiencies. Fig. 20 compares simulated and experimental power outputs to differences in generator efficiency throughout the 70%–90% range. The highest simulated power is 364.76 watts at a generator efficiency of 90%. While the smallest is 283.70 watts at a generator with 70% efficiency, the power from the simulation results did not differ significantly from the power generated by the experiment, which was 294.19 watts.

Table 7. Differences in electrical power between experiment and simulation

Generator efficiency (%)	Simulation (watts)	Experiment (watts)	% Differences (absolute)
90	364.76	294.19	23.99
87.5	354.62	294.19	20.54
85	344.49	294.19	17.10
82.5	334.36	294.19	13.65
80	324.23	294.19	10.21
77.5	314.09	294.19	6.77
75	303.96	294.19	3.32
72.5	293.83	294.19	0.12
70	283.70	294.19	3.57

The largest discrepancy between the experiment and simulation is 23.99% in generator efficiency of 90%, resulting in a simulation power of 364.76 watts. The smallest difference is 0.12% in generator efficiency of 72.5%, producing a simulated power of 293.83 watts. This result indicates that the difference is still acceptable. Lee *et al.* [49] believe the differences in electrical power output between wind turbine simulations and real-world conditions arise mainly due to variable wind speeds in reality, while simulations often assume steady conditions. Simplified models used in simulations may not fully account for real-world factors like turbulence or blade deformation. Additionally, mechanical losses from friction and inefficiencies in the turbine are often minimized in simulations but can significantly affect actual performance. Consequently, it can be concluded that the wind turbine performance simulation results in this study coincide with the actual condition results. The future works need to evaluate the environmental effects of various turbine designs and operational strategies due to many uncertainties factor in actual condition.

4 Conclusion

The linearization method played a crucial role in simplifying and enhancing the efficiency of the optimization process, which focused on the twist (β) and chord (Cr) distributions along the blade length of the Horizontal Axis Wind Turbine (HAWT). The results demonstrated a significant performance improvement in C_p and mechanical power generated through simulation. Additionally, the manufactured HAWT can generate an average electrical power of 294.19 watts at a rotational speed of 590.66 rpm in real wind conditions. Overall, the linearization method successfully contributed to optimizing the blade profiles by reducing the complexity of the manufacturing process, reducing computational demands, and providing accurate, high-performance blade designs that performed well in both simulations and real wind conditions.

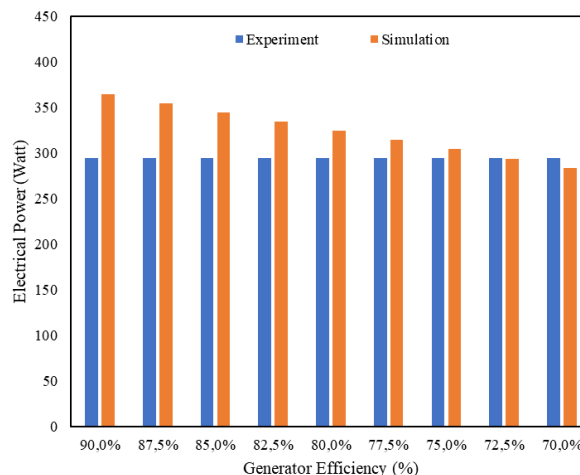


Fig. 20. Comparison of electrical power between experiment and simulation.

The percentage of discrepancy between the simulation and experiment findings is also displayed in Table 7.

Acknowledgment

Authors would like to thank to Institut Teknologi Sumatera for providing the research grant No. 1539be/IT9.2.1/ PT.01.03/ 2024 through “Hibah Penelitian ITERA 2024”. Authors also express gratitude to Lentera Bumi Nusantara for the assistance during research.

References

- [1] EBTKE, “Cadangan Batubara Masih 38,84 Miliar Ton, Teknologi Bersih Pengelolaannya Terus Didorong,” *ebtke.esdm.go.id*, 2021. <https://www.esdm.go.id/id/media-center/arsip-berita/cadangan-batubara-masih-3884-miliar-ton-teknologi-bersih-pengelolaannya-terus-didorong> (accessed Nov. 15, 2023).
- [2] EBTKE, “Potensi Energi Angin Indonesia 2020,” *ebtke.esdm.go.id*, 2021. https://p3tkebt.esdm.go.id/pilot-plan-project/energi_angin/potensi-energi-angin-indonesia-2020
- [3] H. Piggott, “Windpower workshop: building your own wind turbine,” *Wind. Work. Build. your own Wind turbine*, 1997.
- [4] A. Albanesi, V. Fachinotti, I. Peralta, B. Storti, and C. Gebhardt, “Application of the inverse finite element method to design wind turbine blades,” *Compos. Struct.*, vol. 161, pp. 160–172, 2017, doi: 10.1016/j.compstruct.2016.11.039.
- [5] A. A. Nada and A. S. Al-Shahrani, “Shape Optimization of Low Speed Wind Turbine Blades using Flexible Multibody Approach,” *Energy Procedia*, vol. 134, pp. 577–587, 2017, doi: 10.1016/j.egypro.2017.09.567.
- [6] E. Musyarofah, “Rancang Bangun Sudu Inverse Taper Pada Small Wind Turbine Dengan Tipe Airfoil Sg6042,” 2020.
- [7] A. DWI SAPTO and H. PANDU RUMAKSO, “Uji Coba Performa Bentuk Airfoil Menggunakan Software Qblade Terhadap Turbin Angin Tipe Sumbu Horizontal,” *J. Tek. Mesin*, vol. 10, no. 1, p. 1, 2021, doi: 10.22441/jtm.v10i1.10212.

- [8] S. N. Wahyudi, D. H. Al-Janani, and D. D. Saputro, "Konfigurasi Bilah NACA 3612 Terhadap Performa Turbin Angin Sumbu Horizontal (TASH)," *J. Rekayasa Mesin*, vol. 11, no. 3, pp. 415–425, 2020, doi: 10.21776/ub.jrm.2020.011.03.14.
- [9] M. A. Ikaningsih and W. Rosihan, "Penggunaan Styrofoam sebagai Material Bilah Turbin Angin," *Rotasi*, vol. 21, no. 1, p. 23, 2019, doi: 10.14710/rotasi.21.1.23-29.
- [10] M. A. Cahyono and L. Laksamana, "Pull and Bending Force Carbon Fiber Composite," *Vortex*, vol. 1, no. 2, p. 87, 2021, doi: 10.28989/vortex.v1i2.899.
- [11] W. T. Nugroho, "Pengaruh Model Serat Pada Bahan Fiberglass Terhadap Kekuatan, Ketangguhan, Dan Kekerasan Material," *J. Ilm. Inov.*, vol. 15, no. 1, 2016, doi: 10.25047/jii.v15i1.58.
- [12] S. K. Lapeantu, A. Hapid, and Muthmainnah, "Sifat Mekanika Kayu Pinus (Pinus merkusii Jungh et de Vriese) Asal Desa Taende Mori Atas Morowali Utara Sulawesi Tengah," *J. War. Rimba*, vol. 5, pp. 121–126, 2017.
- [13] A. Wijayanto, S. Dumarçay, C. Gérardin-Charbonnier, R. K. Sari, W. Syafii, and P. Gérardin, "Phenolic and lipophilic extractives in Pinus merkusii Jungh. et de Vries knots and stemwood," *Ind. Crops Prod.*, vol. 69, pp. 466–471, 2015, doi: 10.1016/j.indcrop.2015.02.061.
- [14] F. N. Rangkuti, M. Rokhmat, and I. N. Zahra, "Perancangan Bilah Taper Pada Turbin Angin Sumbu Horizontal," *eProceedings Eng.*, vol. 8, no. 5, pp. 5834–5842, 2021.
- [15] J. Chen and M. H. Kim, "Review of Recent Offshore Wind Turbine Research and Optimization Methodologies in Their Design," *J. Mar. Sci. Eng.*, vol. 10, no. 1, 2022, doi: 10.3390/jmse10010028.
- [16] M. S. Selig and V. L. Coverstone-Carroll, "Application of a genetic algorithm to wind turbine design," *J. Energy Resour. Technol. Trans. ASME*, vol. 118, no. 1, pp. 22–28, 1996, doi: 10.1115/1.2792688.
- [17] O. Ceyhan, "Aerodynamic Design and Optimization of Horizontal Axis Wind Turbines by Using BEM Theory and Genetic Algorithm," *Aerosp. Eng.*, 2008.
- [18] X. Liu, Y. Chen, and Z. Ye, "Optimization model for rotor blades of horizontal axis wind turbines," *Front. Mech. Eng. China*, vol. 2, no. 4, pp. 483–488, 2007, doi: 10.1007/s11465-007-0084-9.
- [19] A. Abbaskhah, H. Sedighi, P. Akbarzadeh, and A. Salavatipour, "Optimization of horizontal axis wind turbine performance with the dimpled blades by using CNN and MLP models," *Ocean Eng.*, vol. 276, 2023, doi: 10.1016/j.oceaneng.2023.114185.
- [20] A. Sedaghat, M. Mirhosseini, and M. Moghimi Zand, "Energy Equipment and Systems Aerodynamic design and economical evaluation of site specific horizontal axis wind turbine (HAWT)," *Energyequipsys*, vol. 2, pp. 43–55, 2014.
- [21] R. Özkan and M. S. Genç, "Aerodynamic design and optimization of a small-scale wind turbine blade using a novel artificial bee colony algorithm based on blade element momentum (ABC-BEM) theory," *Energy Convers. Manag.*, vol. 283, 2023, doi: 10.1016/j.enconman.2023.116937.
- [22] J. Xu *et al.*, "A cost-effective CNN-BEM coupling framework for design optimization of horizontal axis tidal turbine blades," *Energy*, vol. 282, 2023, doi: 10.1016/j.energy.2023.128707.
- [23] S. A. Kale and R. N. Varma, "Aerodynamic design of a horizontal axis micro wind turbine blade using NACA 4412 profile," *Int. J. Renew. Energy Res.*, vol. 4, no. 1, pp. 69–72, 2014.
- [24] V. Keshavarzadeh, R. G. Ghanem, and D. A. Tortorelli, "Shape optimization under uncertainty for rotor blades of horizontal axis wind turbines," *Comput. Methods Appl. Mech. Eng.*, vol. 354, pp. 271–306, 2019, doi: 10.1016/j.cma.2019.05.015.
- [25] S. Rahgozar, A. Pourrajabian, S. A. A. Kazmi, and S. M. R. Kazmi, "Performance analysis of a small horizontal axis wind turbine under the use of linear/nonlinear distributions for the chord and twist angle," *Energy Sustain. Dev.*, vol. 58, pp. 42–49, 2020, doi: 10.1016/j.esd.2020.07.003.
- [26] A. M. Abdelsalam, W. A. El-Askary, M. A. Kotb, and I. M. Sakr, "Experimental study on small scale horizontal axis wind turbine of analytically-optimized blade with linearized chord twist angle profile," *Energy*, vol. 216, 2021, doi: 10.1016/j.energy.2020.119304.
- [27] B. Augustiantyo, R. Setiawan, and O. Oleh, "Optimasi Desain Bilah Dengan Metode Linearisasi Chord Dan Twist Terhadap Performa Turbin Angin Sumbu Horizontal," *Media Mesin Maj. Tek. Mesin*, vol. 22, no. 2, pp. 97–110, 2021, doi: 10.23917/mesin.v22i2.14712.
- [28] R. B. Marten, David; Saverin, Joseph; de Luna, "Theory Guide: Blade Element Momentum Method," 2021. <https://docs.qblade.org/src/theory/aerodynamics/bem/bem.html> (accessed Dec. 12, 2023).
- [29] M. R. Islam, L. Bin Bashar, and N. S. Rafi, "Design and Simulation of A Small Wind Turbine Blade with Qblade and Validation with MATLAB," *2019 4th Int. Conf. Electr. Inf. Commun. Technol. EICT 2019*, 2019, doi: 10.1109/EICT48899.2019.9068762.
- [30] M. Yamin and Z. Alkahfi Raamadhan, "Neural Network Approach for Predicting Aerodynamic Performance of NACA Airfoil at Low Reynolds Number," *Desiminating Inf. Res. Mech. Eng. Polimesin*, vol. 20, no. 2, p. 2022, 2022.
- [31] I. N. Zahra, "Dasar-Dasar Perancangan Bilah," pp. 13–19, 2020.
- [32] R. Vallinayagam, S. Vedharaj, W. M. Yang, P. S. Lee, K. J. E. Chua, and S. K. Chou, "Combustion performance and emission characteristics study of pine oil in a diesel engine," *Energy*, vol. 57, pp. 344–351, 2013, doi: 10.1016/j.energy.2013.05.061.
- [33] D. T. Kashid, A. K. Parkhe, S. M. Kale, S. S. Wangikar, C. C. Jadhav, and H. N. Paricharak, "NACA 4415 Aerofoil: Numerical Analysis for Performance in Drag and Lift," *Techno-societal 2022*, pp. 461–474, 2024, doi: 10.1007/978-3-031-34644-6_48.
- [34] C. Pranesh, M. Sivapragasam, M. D. Deshpande, and H. K. Narahari, "Negative lift characteristics of NACA 0012 aerofoil at low Reynolds numbers," *Sadhana - Acad. Proc. Eng. Sci.*, vol. 44, no. 1, 2019, doi: 10.1007/s12046-018-1008-6.
- [35] P. R. Mehta and R. V. Kale, "Parameters Affecting Design of Wind Turbine Blade—A Review," *Lect. Notes Mech. Eng.*, pp. 315–324, 2022, doi: 10.1007/978-981-16-7909-4_28.
- [36] B. Xu, Z. Li, Z. Zhu, X. Cai, T. Wang, and Z. Zhao, "The Parametric Modeling and Two-Objective Optimal Design of a Downwind Blade," *Front. Energy Res.*, vol. 9, 2021, doi: 10.3389/fenrg.2021.708230.
- [37] Y. D. Herlambang *et al.*, "Optimization of savonius turbine towards different inner blade positions to improve turbine performance," *J. Polimesin*, vol. 21, no. 1, pp. 2023–2026, 2023.
- [38] H. Zhang, Y. Hu, and W. Wang, "Wind tunnel experimental study on the aerodynamic characteristics of straight-bladed vertical axis wind turbine," *Int. J. Sustain. Energy*, vol. 43, no. 1, 2024, doi: 10.1080/14786451.2024.2305035.
- [39] O. C. Castillo, V. R. Andrade, J. J. R. Rivas, and R. O. González, "Comparison of Power Coefficients in Wind Turbines Considering the Tip Speed Ratio and Blade Pitch Angle," *Energies*, vol. 16, no. 6, 2023, doi: 10.3390/en16062774.

- [40] A. A. Firoozi, F. Hejazi, and A. A. Firoozi, "Advancing Wind Energy Efficiency: A Systematic Review of Aerodynamic Optimization in Wind Turbine Blade Design," *Energies*, vol. 17, no. 12, 2024, doi: 10.3390/en17122919.
- [41] W. Hao, A. Abdi, G. Wang, and F. Wu, "Study on the Pitch Angle Effect on the Power Coefficient and Blade Fatigue Load of a Vertical Axis Wind Turbine," *Energies*, vol. 16, no. 21, 2023, doi: 10.3390/en16217279.
- [42] L. Li, I. Chopra, W. Zhu, and M. Yu, "Performance analysis and optimization of a vertical-axis wind turbine with a high tip-speed ratio," *Energies*, vol. 14, no. 4, 2021, doi: 10.3390/en14040996.
- [43] A. Alkhabbaz, H. S. Yang, A. H. S. Weerakoon, and Y. H. Lee, "A novel linearization approach of chord and twist angle distribution for 10 kW horizontal axis wind turbine," *Renew. Energy*, vol. 178, pp. 1398–1420, 2021, doi: 10.1016/j.renene.2021.06.077.
- [44] R. Syahputra, A. Jamal, S. Sudarisman, K. Purwanto, and I. Soesanti, "Performance Investigation of Standalone Wind Power System Equipped with Sinusoidal Pwm Power Inverter for Household Consumer in Rural Areas of Indonesia," *SSRN Electron. J.*, 2021, doi: 10.2139/ssrn.3940884.
- [45] I. Ifanda *et al.*, "Optimizing Turbine Siting and Wind Farm Layout in Indonesia," *Int. J. Renew. Energy Res.*, vol. 13, no. 3, pp. 1351–1363, 2023, doi: 10.20508/ijrer.v13i3.14070.g8806.
- [46] D. G. Cendrawati, N. W. Hesty, B. Pranoto, Aminuddin, A. H. Kuncoro, and A. Fudholi, "Short-Term Wind Energy Resource Prediction Using Weather Research Forecasting Model for a Location in Indonesia," *Int. J. Technol.*, vol. 14, no. 3, pp. 584–595, 2023, doi: 10.14716/ijtech.v14i3.5803.
- [47] A. N. Robertson, K. Shaler, L. Sethuraman, and J. Jonkman, "Sensitivity analysis of the effect of wind characteristics and turbine properties on wind turbine loads," *Wind Energy Sci.*, vol. 4, no. 3, pp. 479–513, 2019, doi: 10.5194/wes-4-479-2019.
- [48] B. M. Mazetto and T. G. Ritto, "Uncertainty and Global Sensitivity Analysis of Wind Turbines Fatigue in Non-ideal Conditions," *J. Vib. Eng. Technol.*, vol. 10, no. 6, pp. 2391–2402, 2022, doi: 10.1007/s42417-022-00632-7.
- [49] J. C. Y. Lee *et al.*, "The Power Curve Working Group's assessment of wind turbine power performance prediction methods," *Wind Energy Sci.*, vol. 5, no. 1, pp. 199–223, 2020, doi: 10.5194/wes-5-199-2020.